Supplementary Information

Impact of Solvent Sulfolane in Enhancing Methanol Selectivity During Methane Partial Oxidation on Fe-ZSM-5 Catalyst with H_2O_2 as Oxidant

B. Sathya Sai Rengam, Pushkala Venkatesh and Jithin John Varghese*

Department of Chemical Engineering, Indian Institute of Technology Madras, Chennai 600036

*Email: jithinjv@iitm.ac.in

S1. Computational methods and simulation systems

S.1.1. Sulfolane forcefield reparameterization

The existing Generalized Amber Force Field (GAFF) for sulfolane reported by Caleman et al.[1] was used to compute and compare against the bulk properties of sulfolane such as density [2], dielectric constant [3], and dipole moment [4]. Large deviations from the reported experimental values were observed for all the properties as seen from Table S1.

Table S1. Comparison of bulk properties of sulfolane computed from classical molecular dynamics simulations with forcefield parameters previously available in the literature and after re-parameterization, against the experimental data at 323 K and 1 bar pressure.

Bulk Property	Experimental data	Ref.	Properties calculated with existing forcefield [1]	Properties calculated with optimized forcefield
Density (kg/m^3)	1244.21	2	1296.90	1243.18 ± 7.90
Dielectric constant (Debye)	40.76	3	22.22	38.46
Dipole moment(μ)	4.69	4	6.14	6.23 ± 0.19

Hence re-optimization of the forcefield parameters was done, especially by modifying the Lennard-Jones (LJ) parameters and the partial charges on the atoms of sulfolane. Re-parameterization of the partial charges on the atoms of sulfolane (refer to Figure S1 for molecular representation and atom numbering) was done by obtaining Electrostatic Potential (ESP) based atomic charges of sulfolane from Density Functional Theory calculations in GAUSSIAN 16[5] with the B3LYP[6,7] exchange correlation functional and the 6-311+g(d,p) basis set.

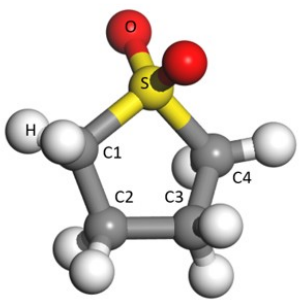

Figure S1. The molecular representation of the sulfolane molecule with atomic indices corresponding to data in Table S2.

The obtained ESP charges on carbon, hydrogen, sulfur, and oxygen atoms of the sulfolane molecule were optimized as provided in Table S2 to obtain a good fit of the computed bulk properties with the experimental data. Parameters for LJ potentials (used for calculating non-bonded interactions) were also modified along with charges on atoms of sulfolane and the final optimized values are as reported in Table S2.

Table S2. Optimized partial charges and Lennard-Jones parameters for all the atoms of sulfolane molecule.

Atom	**Partial charges (e)**	**σ (nm)**	**ε_{ij} (kJ/mole)**
Sulfur	0.800	0.355	1.046
Oxygen	-0.531	0.296	0.711
C1, C4 (attached to sulfur)	-0.135	0.350	0.276
Hydrogens (attached to C1, C4)	0.096	0.250	0.125
C2, C3	-0.020	0.350	0.276
Hydrogens (attached to C2, C3)	0.047	0.250	0.125

S.1.2. Simulation systems used in classical molecular dynamics simulations.

Table S3. The number of methane, methanol, hydrogen peroxide, water, and sulfolane molecules considered for the classical molecular dynamics simulations to compute the diffusion coefficient of methane, methanol, and hydrogen peroxide for pure water, pure sulfolane system and mixture of sulfolane with aqueous H_2O_2.

System	Number of CH_4	Number of CH_3OH	Number of H_2O_2	Number of water	Number of sulfolane
Diffusion of CH_4 in water	3	-	149	3031	-
Diffusion of CH_4 in sulfolane (Pure H_2O_2)	61	-	149	-	579
Diffusion of CH_4 in sulfolane (30 wt% H_2O_2)	61	-	149	653	579
Diffusion of CH_3OH in water	-	8	149	3031	-
Diffusion of CH_3OH in sulfolane (Pure H_2O_2)	-	8	149	-	579
Diffusion of CH_3OH in sulfolane (30 wt% H_2O_2)	-	8	149	653	579
Diffusion of H_2O_2 in water	-	-	149	3031	-
Diffusion of H_2O_2 in sulfolane (Pure H_2O_2)	-	-	149	-	579
Diffusion of H_2O_2 in sulfolane (30 wt% H_2O_2)	-	-	149	653	579

The number of molecules of each species in the simulation systems considered in water and sulfolane solvent is shown in Table S3. The number of molecules of water and sulfolane considered for each simulation is based on the density of the respective solvents in a 4.5 nm simulation box. The number of H_2O_2 and methanol molecules considered was based on the concentration of the oxidant (pure H_2O_2 and 30 wt% H_2O_2) and product yield respectively, reported in the literature.[8] The choice of the number of molecules of methane in water and sulfolane was according to the solubility in each of the respective solvents.[9,10] All the simulations are with the presence of H_2O_2 which is the oxidant present in the system.

S2. Results

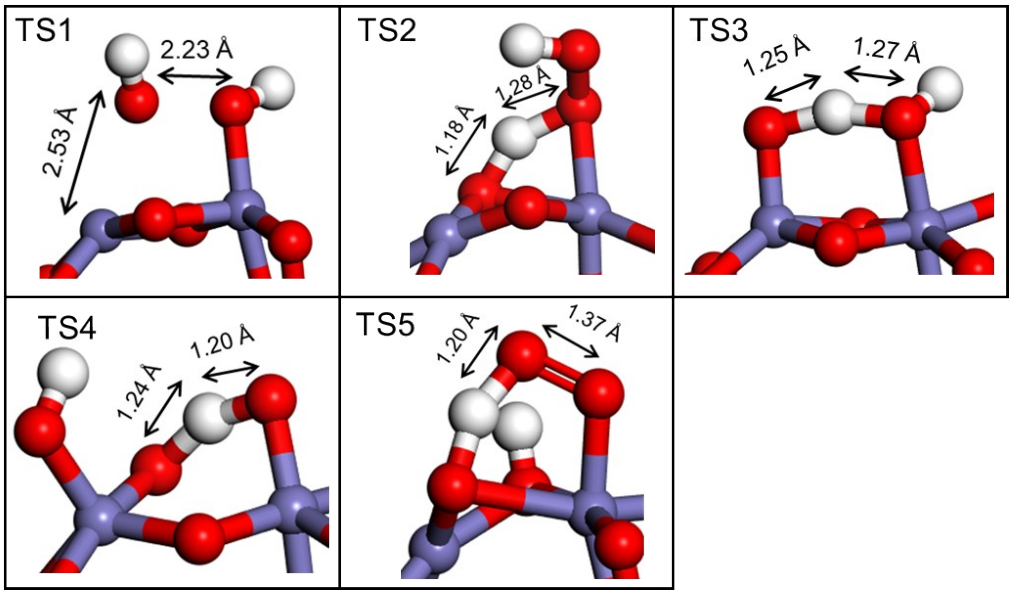

Figure S2 The transition states for the different elementary steps involved in the active species formation by oxidant H_2O_2 dissociation at the $[Fe_2(\mu_2\text{-}O)_2]^{2+}$ active site in Fe-ZSM-5 catalyst as shown in Figure 2 of the manuscript. The sulfolane molecules coordinated to the Fe atoms are not shown for clarity. Colour code: O, Fe, C, and H are red, purply-blue, ash and white spheres, respectively.

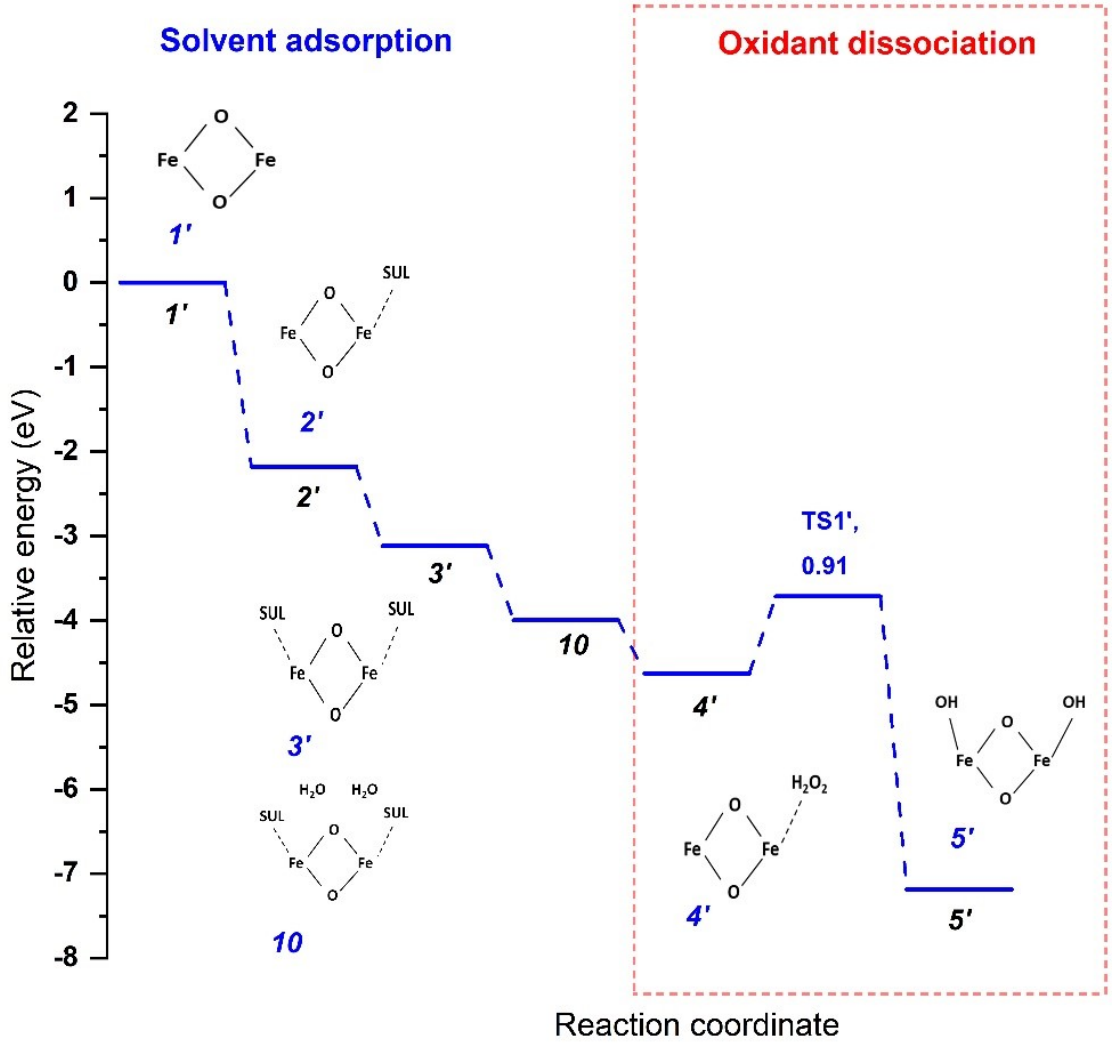

Figure S3. Energy profile for sulfolane and water (mixture of solvents) coordination with the binuclear [$Fe_2(\mu_2\text{-}O)_2$] active site in Fe-ZSM-5 catalyst and active oxygen species formation from H_2O_2 dissociation. The solvent molecules coordinated to the Fe atoms are not shown for clarity in the intermediates beyond 10 along the reaction coordinate.

Studies with free solvent molecules (mixture of solvents) need to be performed systematically and the results are to be interpreted cautiously, as the impact of the presence of a few arbitrary solvent molecules which are not representative of the condensed phased environment in the calculated energy profiles could be large. Nevertheless, to understand the trend of impact of water from the aqueous H_2O_2 solution that is typically used in the experiments, we investigated H_2O_2 dissociation and methane activation to form methanol in the presence of water molecules in the ZSM-5 pores. A simulation system comprising two water molecules (one close to each Fe atom in the pore) in addition to the coordinated sulfolane was considered (Intermediate 10 in Figure S3). The activation barrier for the homolytic dissociation of H_2O_2 and formation of two Fe-OH was not impacted significantly by the presence of water (activation barrier of 0.91 eV compared to 0.96 eV without the water molecules) but the formation was substantially more stable in the solvent mixture as can be seen in Figure S3. The heterolytic dissociation to form Fe-OOH was significantly less favourable than in the pure sulfolane solvent.

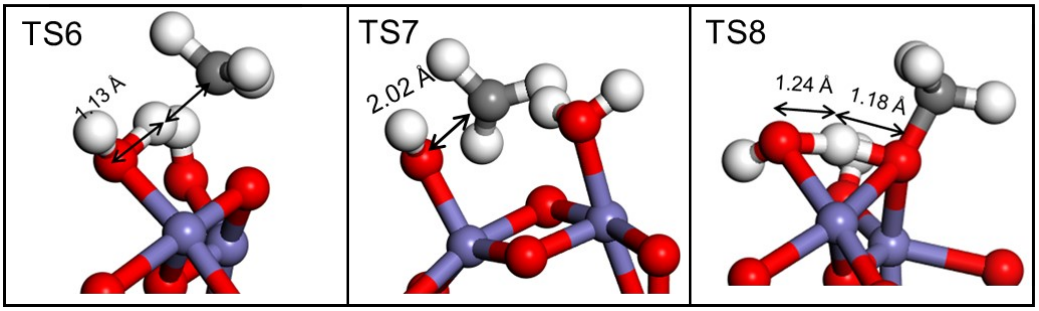

Figure S4. The transition states for the different elementary steps involved in the methane activation and methanol formation by the direct and indirect pathways on [OH-Fe(μ-O)$_2$Fe-OH] active site in Fe-ZSM-5 catalyst, corresponding to the energy profile shown in Figure 3 of the manuscript. The sulfolane molecules coordinated to the Fe atoms are not shown for clarity. Colour code of atoms is the same as in Figure S2.

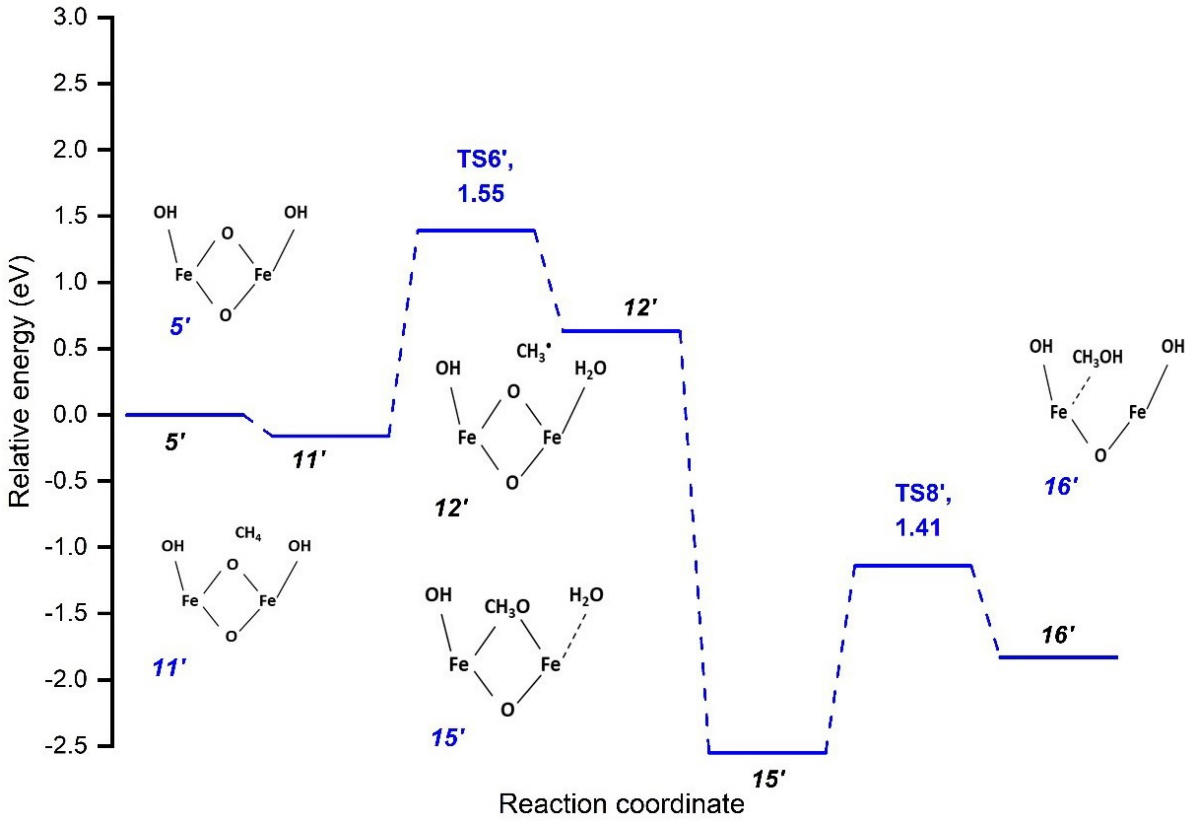

Figure S5. Energy profile for methane activation and methanol formation on [OH-Fe(μ-O)$_2$Fe-OH] active site in Fe-ZSM-5 catalyst in presence of both sulfolane and water (mixture of solvents). Blue line represents methanol formation via indirect pathway. The solvent molecules (2 sulfolane and 2 water) coordinated to the Fe atoms are not shown for clarity.

To understand the potential impact of water from the aqueous H_2O_2 solution that is typically used in the experiments, methane activation and formation of methanol was investigated in the presence of two water molecules in addition to the two sulfolane molecules in the ZSM-5 pores. The barrier for the first C-H bond activation of methane to form the methyl radical was

reduced to 1.55 eV compared to 1.79 eV in pure sulfolane. The formed species (CH_3 radical and methoxy species) were substantially more stable in the solvent mixture than pure sulfolane as shown in Figure S5. Overall, these energy trends indicate the possibility of higher reactivity and methanol formation in the mixed solvent than pure sulfolane and this is in agreement with the trends reported for methane partial oxidation on Fe-MFI catalyst with mixed sulfolane-water solvent in the literature.[8]

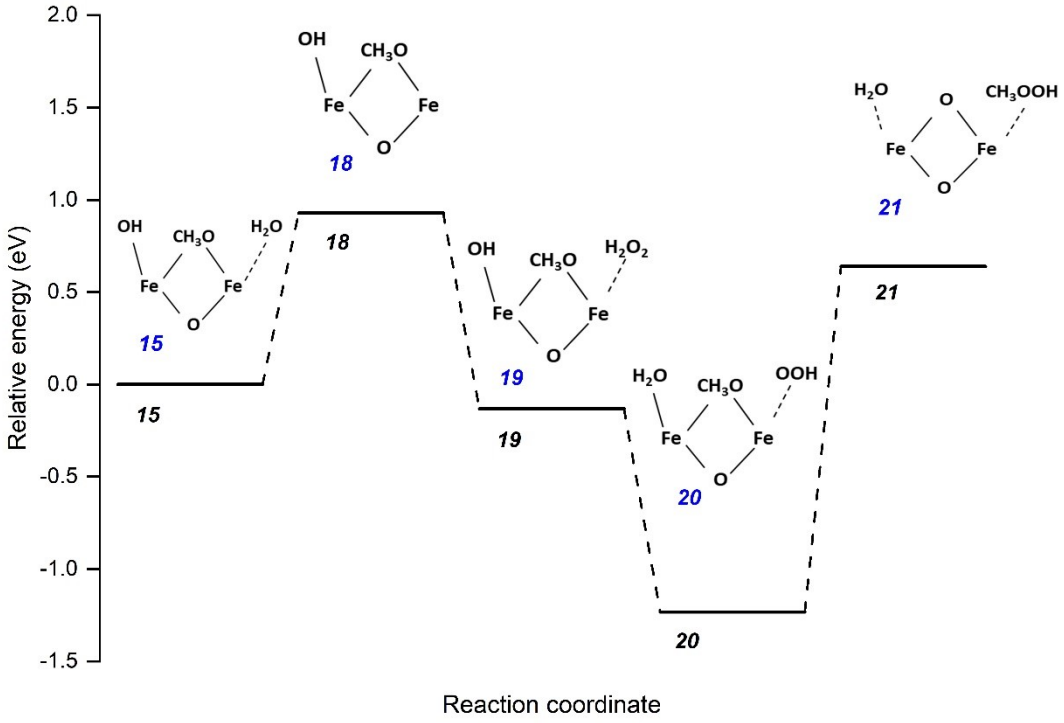

Figure S6. Energy profile for methyl peroxide formation from methoxy species on [OH-Fe(μO)$_2$Fe-OH] active site in Fe-ZSM-5 catalyst.

Methyl peroxide can form from methoxy species if an OOH active oxygen species forms on the active site. Water removal from intermediate 15 in Figure S6, followed by H_2O_2 adsorption (intermediate 19) can result in its dissociation into Fe-OOH and water (intermediate 20). However, the migration of the methyl radical from the bridged oxygen to the Fe-OOH to form methyl peroxide (intermediate 21) was highly unfavourable (reaction energy= 1.87 eV). Hence, the formation of the methyl peroxide is likely to be negligible in a sulfolane environment.

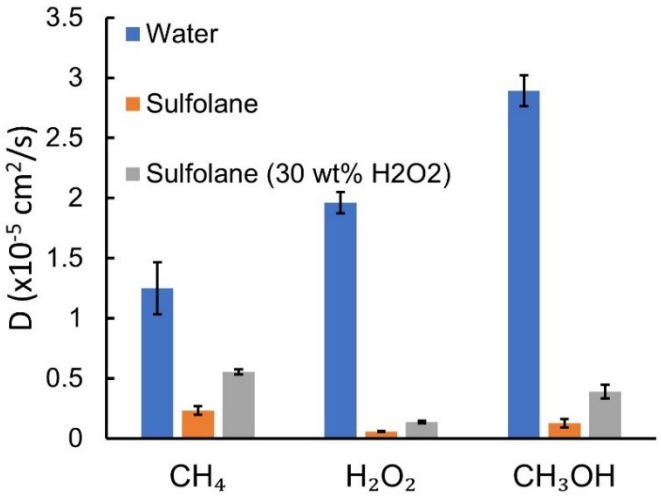

Figure S7. Comparison of computed diffusion coefficient of CH_4, H_2O_2, and CH_3OH in water, sulfolane and sulfolane with 30 wt.% aqueous H_2O_2 solution from classical molecular dynamics simulations performed at 323 K and 30 bar pressure. Refer to Table S3 for description of the simulation systems.

The diffusion coefficient of the reactants and the product is substantially higher with the presence of small amounts of water (from aqueous H_2O_2 solution) than in pure sulfolane, although each of these are much smaller than in pure water. These, together with the influence of water in sulfolane on reaction kinetics (Figures S3 and S5), point towards an increase in methanol yield in the presence of water with sulfolane (mixed solvent). This is consistent with the high yield of methanol reported by Yokoi and co-workers[8] on Fe-MFI catalyst with sulfolane- water mixture and H_2O_2 oxidant. However, a further detailed study would be necessary to quantify the impact of the mixed solvent on catalytic performance enhancement and to identify a solvent composition for highest yield of methanol.

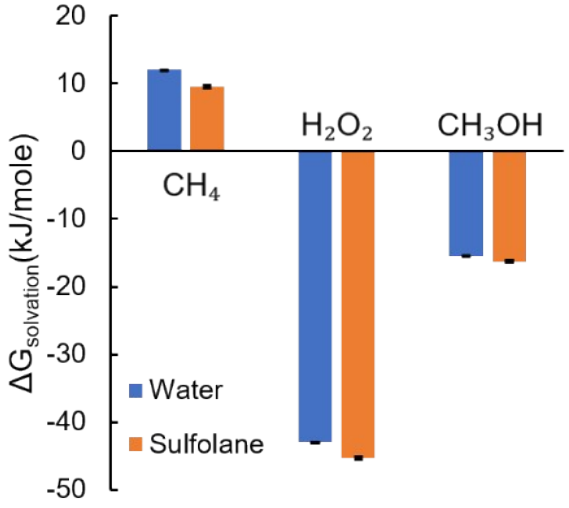

Figure S8. Computed solvation-free energy of CH_4, H_2O_2, and CH_3OH in water and sulfolane from classical molecular dynamics simulations performed at 323 K and 30 bar pressure. Refer to Table S3 for details on the simulation systems.

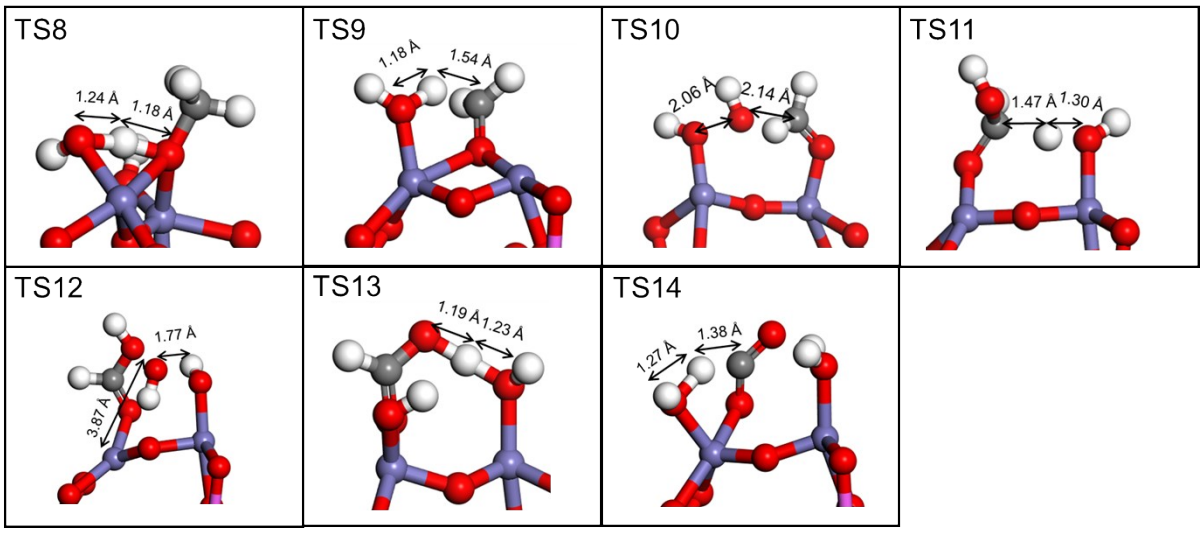

Figure S9. The transition states for the different elementary steps involved in the oxidation of methoxy species formed on [OH-Fe(μ-O)$_2$Fe-OH] active site in Fe-ZSM-5 catalyst, corresponding to the energy profile shown in Figure 5 of the manuscript. The sulfolane molecules coordinated to the Fe atoms are not shown for clarity. Colour code of atoms is the same as in Figure S2.

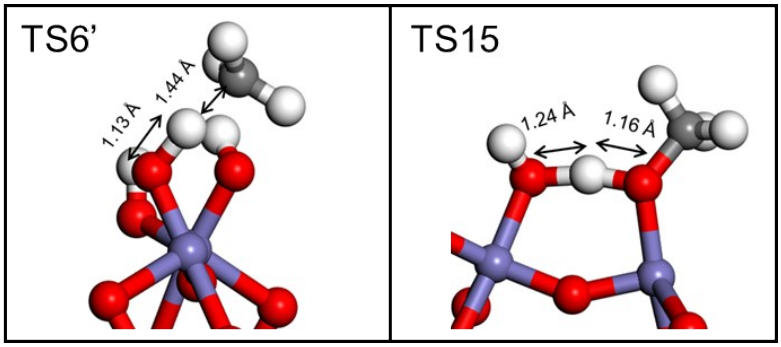

Figure S10. The transition states for the different elementary steps involved in the methane activation pathway on [Fe=O] of [(OH)$_2$Fe(μ-O)Fe=O] active site of Fe-ZMS-5 catalyst. The sulfolane molecules coordinated to the Fe atoms are not shown for clarity. Colour code of atoms is the same as in Figure S2.

References

1 C. Caleman, P. J. van Maaren, M. Hong, J. S. Hub, L. T. Costa and D. van der Spoel, *J. Chem. Theory. Comput.*, 2012, **8**, 61–74.

2 M. A. Saleh, M. Shamsuddin Ahmed and S. K. Begum, *Phys. Chem. Liquids*, 2006, **44**, 153–165.

3 J. F. Casteel and P. G. Sears, *J. Chem. Eng. Data*, 1974, **19**, 196–200.

4 U. Tilstam, *Org. Process Res. Dev.*, 2012, **16**, 1273–1278.

5 M. J. Frisch, G. W. Trucks, H. B. Schlegel, G. E. Scuseria, M. A. Robb, J. R. Cheeseman, G. Scalmani, V. Barone, G. A. Petersson, H. Nakatsuji, X. Li, M. Caricato, A. v Marenich, J. Bloino, B. G. Janesko, R. Gomperts, B. Mennucci, H. P. Hratchian, J. v Ortiz, A. F. Izmaylov, J. L. Sonnenberg, D. Williams-Young, F. Ding, F. Lipparini, F. Egidi, J. Goings, B. Peng, A. Petrone, T. Henderson, D. Ranasinghe, V. G. Zakrzewski, J. Gao, N. Rega, G. Zheng, W. Liang, M. Hada, M. Ehara, K. Toyota, R. Fukuda, J.

Hasegawa, M. Ishida, T. Nakajima, Y. Honda, O. Kitao, H. Nakai, T. Vreven, K. Throssell, J. A. Montgomery Jr., J. E. Peralta, F. Ogliaro, M. J. Bearpark, J. J. Heyd, E. N. Brothers, K. N. Kudin, V. N. Staroverov, T. A. Keith, R. Kobayashi, J. Normand, K. Raghavachari, A. P. Rendell, J. C. Burant, S. S. Iyengar, J. Tomasi, M. Cossi, J. M. Millam, M. Klene, C. Adamo, R. Cammi, J. W. Ochterski, R. L. Martin, K. Morokuma, O. Farkas, J. B. Foresman and D. J. Fox, Gaussian 16 Revision B.01. 2016; 2016 Gaussian Inc. Wallingford CT.

6 A. D. Becke, *J. Chem. Phys.*, 1993, **98**, 5648–5652.

7 C. Lee, W. Yang and R. G. Parr, *Phys. Rev. B*, 1988, **37**, 785.

8 P. Xiao, Y. Wang, T. Nishitoba, J. N. Kondo and T. Yokoi, *Chem. Commun.*, 2019, **55**, 2896–2899.

9 F. Jou, R. D. Deshmukh, F. D. Otto and A. E. Mather, *Fluid. Phase Equilib.* 1990, ***56***, 313–324.

10 Z. Duan, N. Møller, J. Greenberg and J. H. Weare, *Geochim. Cosmochim. Acta* 1992, ***56***, 1451–1460.